OPTIMIZED DESIGN OF A TWO-DEGREE-OF-FREEDOM POSITION SERVO SYSTEM BASED ON FRACTIONAL-ORDER ACTIVE DISTURBANCE REJECTION CONTROL

Zhengkun GUO[1, *], Zhicheng ZHAO[2], Ziying ZHANG[1, 3]

This research introduced an optimized method based on two-degree-of-freedom fractional-order active disturbance rejection control (FOADRC) to improve the control performance of position servo systems. Proportional-Integral-Derivative (PID) and active disturbance rejection control (ADRC) techniques, the developed method incorporated fractional-order filters with a two-degree-of-freedom control strategy and refined nonlinear functions within extended state observer (ESO). This combination significantly improved the dynamic response and robustness of the system. Simulation results indicated that the proposed approach exceled in decreasing overshoot, minimizing steady-state error, and shortening response time. Notably, it demonstrated superior robustness under complex operating conditions. In addition, the proposed strategy not only simplified the parameter tuning process of the controller, but also showed promising potential for practical engineering applications.

Keywords: Fractional-order control; Self-disturbance rejection control; Position servo system; Two-degree-of-freedom control

1. Introduction

Position servo systems are extensively applied in modern industry[1]. By increasing demand for manufacturing due to the increasing demands for higher manufacturing precision and faster response speeds, enhancement the control performance of servo systems has become a critical issue that needs to be addressed urgently. Currently, proportional-integral-derivative (PID) controllers are the primary option for practical motor control systems[2]. Although traditional PID control methods are easy to implement, they suffer from limitations such as slow response speeds and weak disturbance rejections under complex operating conditions[3].

* Corresponding author
[1] Department of Mechanical and Electrical Engineering, Shanxi Institute of Energy, Jinzhong 030600, Shanxi, China, gzk2025@sxie.edu.cn
[2] School of Electronic Information Engineering, Taiyuan University of Science and Technology, Taiyuan 030024, Shanxi, China
[3] School of Mechanical and Information Engineering, China University of Mining and Technology-Beijing, Beijing 100083, China

Active disturbance rejection control (ADRC) enhances system robustness by compensating for both internal and external disturbances. Various research works have been conducted on this topic. For instance, Li et al. developed a sliding mode ADRC (SM-ADRC) method[4]; Ibrahim et al. combined conventional particle swarm optimization algorithm with linear ADRC (LADRC) to enhance the charging capability of photovoltaic systems[5]; Luo et al. applied LADRC to replace traditional PI control loops, effectively filtering out the DC component of the grid under non-ideal conditions[6]; Wu et al. used ADRC to improve aircraft performance[7]; and Yuhang et al. developed an improved ADRC algorithm to enhance the heading control of unmanned aerial vehicles under the disturbances of wind and wave [8]. Furthermore, Alatawi et al. integrated a two-degree-of-freedom control strategy to further enhance the target tracking and disturbance rejection capabilities of the system[9]. In magnetic field compensation systems, a noise suppression technique incorporating a time-delay variable and a second-order coupled model obtained a performance improvement of 27.5% compared to conventional methods [10]. ADRC strategy in cooling control for lithium-ion battery packs obtained higher energy efficiency and temperature control precision by balancing dynamic response with steady-state accuracy [11]. In pressurizer control for nuclear power plants, the developed method was found to be effective under disturbance conditions, presenting better setpoint tracking and disturbance rejection performance than optimized PID control [12]. Regarding exoskeleton control, integration of deep reinforcement learning with ADRC addressed limitations in joint angle and angular velocity feedback, providing a viable solution for intelligent parameter tuning [13]. Application of cascade observers significantly enhanced noise suppression and response speed of steady-state and dynamic control of turbofan engines, creating greater robustness under complex flight environments [14]. However, since most existing filters are designed according to integer-order methods, striking a balance between dynamic performance and robustness is difficult, particularly under high-precision control requirements.

Recently, fractional-order control methods have gradually become very popular among researchers. Fractional calculus provides a powerful framework for modeling complex systems with memory effects, finding applications across various scientific fields. For instance, it has been used to model the decay of a potential vortex in fluid dynamics [14] and to analyze and optimize the control of fractional damped oscillatory systems [15]. Furthermore, fractional derivatives can enhance signal processing techniques, such as the development of a fractional-order Teager Kaiser Energy Operator for improved fault diagnosis in rotating machinery [17]. These examples highlight how fractional-order approaches can lead to more accurate physical models and improved performance in control and diagnostic applications. Compared with traditional integer-order controllers, fractional-order controllers offer a wider range of parameter tuning and more flexible dynamic

performance adjustment possibilities. Continuous technological progress and interdisciplinary integrations drive control schemes to further address disturbances and parameter uncertainties, thereby improving robust control designs. However, existing methods still face challenges such as complex parameter tuning and insufficient robustness in practical applications.

To address these challenges, this research proposed an optimized method based on two-degree-of-freedom fractional-order ADRC (FOADRC). This approach significantly improved the dynamic response and disturbance rejection capabilities of the system by combining a fractional-order filter with a two-degree-of-freedom control strategy and refining the nonlinear functions of extended state observer (ESO). In addition, the proposed method simplified the parameter tuning process of the controller, presenting strong potential for practical engineering applications.

2. Mathematical model of position servo system

The structure of the developed position servo system is illustrated in Fig 1.

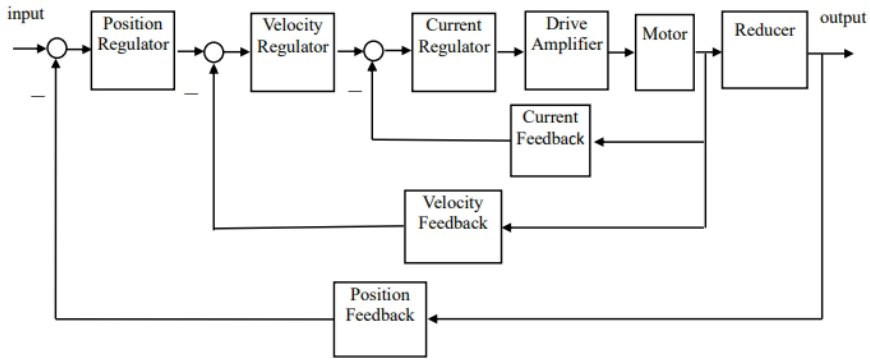

Fig. 1 Structure of the developed position servo system

The Figure illustrates a typical three-loop nested architecture for a position servo system. Its core comprised three regulation loops—position, velocity, and current—which, through multi-level feedback, achieved high-precision and robust motion control. Each loop played a distinct role within the system, forming a hierarchical control structure where response frequencies were progressively increased from the outermost to the innermost loop.

The outermost loop served as the position loop and was responsible for converting input position commands into velocity commands to drive the desired trajectory of the entire system. Since this loop primarily dealt with slowly-varying targets or tasks related to steady-state error correction, it typically employed a relatively simple proportional control strategy. This ensured that the responses were neither overly aggressive, nor insufficiently sensitive, while position feedback mechanism continuously corrected deviations, providing fundamental command

tracking capability to the system. However, due to its limited bandwidth, the ability of the system to respond to rapid dynamic changes predominantly depended on the inner loops.

Velocity loop performed mid-frequency dynamic adjustments by responding to the velocity targets generated by the position loop and correcting any velocity deviations with higher bandwidths. Commonly, this loop is constructed using a PI controller—incorporating an integral component—to improve steady-state precision and disturbance rejection. Velocity feedback provided essential negative feedback during this process, making it possible for the system to provide stronger real-time responses to load disturbances. Acting as a bridge between the input commands and drive system, the dynamic characteristics of this loop directly determined the overall dynamic performance of the system.

Current loop lied at the innermost level, whose function was the precise regulation of the actual current delivered to the drive motor, thereby ensuring immediate and stable torque output. Due to the typical high-frequency responses of current control, this loop was designed with a high bandwidth while considering the hardware constraints of the drive amplifier and motor itself. Through the closed-loop regulation of current feedback, the system could rapidly counteract electrical disturbances or high-frequency dynamic errors, guaranteeing the safe and efficient operation of the drive system.

In summary, the entire system formed a synergistic control network through its nested feedback mechanism. With their faster responses, the inner loops managed high-frequency disturbances, while the outer loops concentrated on steady-state accuracy and trajectory tracking. The integrity of this feedback structure not only enhanced system robustness, but also laid a fundamental groundwork for the integration of various advanced control strategies.

Due to its relatively low cutoff frequency, the velocity loop could be approximated using the following equation as an inertia element in engineering practices:

$$G_s(s) = \frac{k}{Ts+1} \tag{1}$$

where T is the time constant of velocity loop and k is velocity loop gain. The reducer was equivalent to an integral element, represented by $1/K_d$*s, with K_d being reduction ratio. Therefore, the mathematical model of position servo system was expressed as:

$$G_m(s) = \frac{K}{s(Ts+1)} \tag{2}$$

where K is system gain, defined as the ratio of velocity loop gain to reduction ratio.

The developed model characterized the fundamental relationship between system input and output, illustrating the dynamic response characteristics of the system. The frequency response and steady-state performance of the system could be analyzed by using the aforementioned transfer function. This model established the theoretical foundation for subsequent controller design.

3. Controller design

3.1 Fractional-order two-degree-of-freedom internal model control

Due to the limitation of a single adjustable parameter, classical internal model control (IMC) algorithms often struggle to create a balance between dynamic performance and robustness[18]. To solve these problems, this research introduced a fractional-order two-degree-of-freedom internal model control (FO-IMC) strategy. This approach integrated the designs of two independent controllers, with one dedicated to tracking setpoint values and the other to suppressing disturbances, to enhance the dynamic response and disturbance rejection capabilities of the system. The block diagram of the two-degree-of-freedom IMC algorithm is presented in Fig 2.

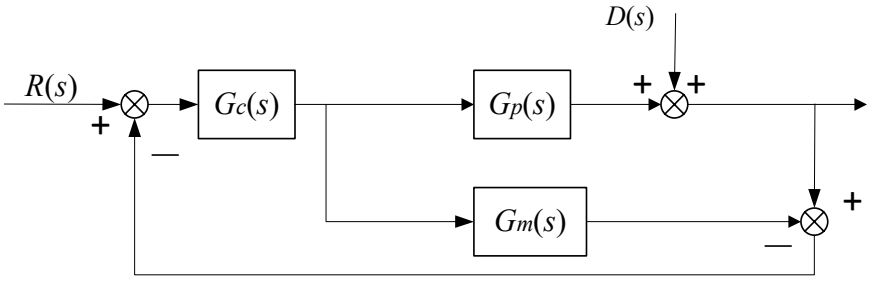

Fig. 2 Structure of the two-degree-of-freedom IMC

In the diagram, $R(s)$ is system input, $Y(s)$ is system output, $D(s)$ is the disturbance affecting the system, $G_{c1}(s)$, $G_{c2}(s)$ are the controllers within the two-degree-of-freedom structure, G_p(s) is the plant being controlled, and $G_m(s)$ is its mathematical model.

The relationship between the $R(s)$ and $Y(s)$ of the system was stated as:

$$Y(s)=\frac{G_{c2}(s)G_p(s)}{1+G_{c1}(s)[G_p(s)-G_m(s)]}R(s)+\frac{1-G_{c1}(s)G_m(s)}{1+G_{c1}(s)[G_p(s)-G_m(s)]}D(s) \tag{3}$$

According to the principles of internal model control, we obtained:

$$G_{c1}(s)=F_1(s)G_{m-}{}^{-1}(s) \tag{4}$$

$$G_{c2}(s) = F_2(s)G_{m\_}^{-1}(s) \tag{5}$$

where $F_1(s)$ and $F_2(s)$ are filters and $G_{m\_}^{-1}(s)$ is minimum-phase part of the controlled model.

Based on these equations, the two-degree-of-freedom internal model control system could be equivalently represented by Fig 3.

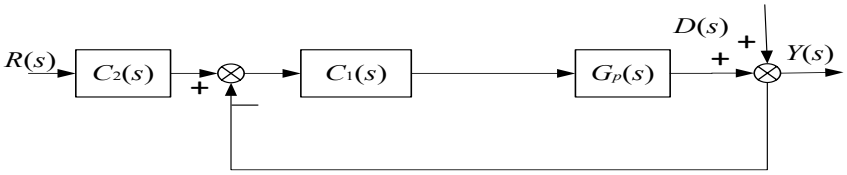

Fig. 3 Equivalent structure of the developed two-degree-of- freedom IMC

The relationship between the input and output of the system was given by:

$$Y(s) = \frac{C_1(s)C_2(s)G_p(s)}{1+C_1(s)G_p(s)}R(s) + \frac{1}{1+C_1(s)G_p(s)}D(s) \tag{6}$$

From Equations (3) and (6), we obtained:

$$C_1(s) = \frac{G_{c1}(s)}{1-G_{c1}(s)G_m(s)} \tag{7}$$

$$C_2 = \frac{G_{c2}(s)}{G_{c1}(s)} \tag{8}$$

The low-pass filters F1(s) and F2(s) in Equations (4) and (5) were defined as:

$$F_1(s) = 1/(1+\lambda_1 s^{\gamma}) \tag{9}$$

$$F_2(s) = 1/(1+\lambda_2 s^{\gamma}) \tag{10}$$

where $1<\gamma<2$ is the order of the filter and $\lambda 1$ and $\lambda 2$ are the time constants of the filters.

The transfer function of the controlled plant was stated as:

$$G_m(s) = \frac{K}{(Ts+1)s} \tag{11}$$

Equation (11) could be approximated as a second-order system, as expressed in Equation (12):

$$G_m(s) = \frac{\beta K}{(Ts+1)(\beta s+1)} \tag{12}$$

where β is a large constant.

From Equations (4), (5), (7), (8), and (9) to (10), we derived:

$$G_{c1} = \frac{(Ts+1)(\beta s+1)}{\beta K(1+\lambda_1 s^{\gamma})} \tag{13}$$

$$G_{c2} = \frac{(Ts+1)(\beta s+1)}{\beta K(1+\lambda_2 s^{\gamma})} \tag{14}$$

$$C_1(s) = \frac{G_{c1}(s)}{1-G_m(s)G_{c1}(s)} = \frac{1}{\beta K\lambda_1 s^{\gamma-1}}\left[(T+\beta)+\frac{1}{s}+\beta Ts\right] \tag{15}$$

$$C_2(s) = \frac{G_{c2}(s)}{G_{c1}(s)} = \frac{1+\lambda_1 S^{\gamma}}{1+\lambda_2 S^{\gamma}} \tag{16}$$

Obviously, C1(s) is a fractional-order PID controller and C2(s) is a fractional-order lead-lag correction link.

3.2 The development of a FOADRC

The ADRC was primarily consisted of a tracking differentiator (TD), an ESO, and a nonlinear state error feedback law (NLSEF). TD was used to organize the transition process of the system, while ESO was responsible for estimating both unknown disturbances and dynamics of the unmodeled components of the plant. These two components were generally adaptable, requiring only parameter setting to cater to different controlled plants. NLSEF in ADRC played a role resembling that of traditional integer-order PID controller, allowing for the substitution of NLSEF with an integer-order PID controller to form a nonlinear PID ADRC, which further enhanced the performance of ADRC. Accordingly, further replacing NLSEF with a fractional-order controller integrated the advantages of both ADRC and fractional-order PID controllers, potentially improving the control quality of the system.

Conventional nonlinear state error feedback function *fal* (e, α, δ) was continuous but not differentiable (i.e., non-smooth) at the origin. For relatively small values of δ, high-frequency chattering might occur with the change of derivatives, which adversely affected control performance. In ADRC, δ was a critical adjustable parameter and its selection added complexity to the controller design. Therefore, constructing a continuous and smooth modified *fal* function was crucial for improving controller robustness.

In traditional ESOs, the *fal*(e, α, δ) function is a continuous power function with an approximately linear segment near the origin and its expression is stated by:

$$fal(e,\alpha,\delta)=\begin{cases}\dfrac{e}{\delta^{\alpha-1}} & |e|\le\delta\\ |e|^{\alpha}\,sign(e) & |e|>\delta\end{cases} \tag{17}$$

where δ is the interval length of the linear segment, e is error signal, and α\alpha is nonlinear factor. The function *sign* (·) denotes the sign function.

The *newfal* function was designed as a continuous and smooth nonlinear function and its mathematical expression was:

$$newfal(e,\alpha,\delta)=\begin{cases}(\alpha-1)\delta^{\alpha-3}e^{3}-(\alpha-1)\delta^{\alpha-2}e^{2}sign(e)+\delta^{\alpha-1}e, & |e|\le\delta\\ |e|^{\alpha}\,sign(e), & |e|>\delta\end{cases} \tag{18}$$

By replacing NLSEF in ADRC with a fractional-order controller and refining the nonlinear function within ESO, a two-degree-of-freedom FOADRC was achieved. The structure of this FOADRC is demonstrated in Fig 4.

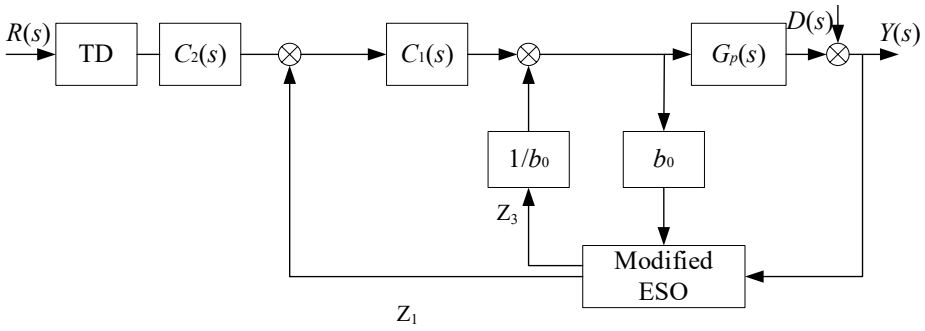

Fig. 4 Two-Degree-of-Freedom FOADRC

The newly designed FOADRC controller integrated the flexibility of fractional-order control while further enhancing the dynamic response and robustness of the system, demonstrating exceptional performance particularly under parameter perturbations and external disturbances.

3.3 Superiority analysis and simulation validation of the newfal function

This section conducted an in-depth comparative analysis on the mathematical characteristics and engineering performance of the nonlinear control function *newfal* within closed-loop systems. This function was specifically designed for improving the non-smoothness issue of the traditional *fal* function in its switching region, particular focusing on its ability to suppress high-frequency chattering. The validation process encompassed both theoretical smoothness analysis at function level and dynamic response simulations under ADRC. Key evaluation criteria included output tracking performance, control signal smoothness, and disturbance estimation quality.

Nonlinear function smoothness plays a critical role in closed-loop control systems. Discontinuities in derivatives often result in sharp fluctuations in controller outputs, directly triggering frequent actuator switching, increasing system energy consumption, and even inducing hardware fatigue failure. Therefore, it is necessary to examine the local mathematical characteristics of *fal* and *newfal* before integrating them into control frameworks.

The function plots and their first derivatives over the interval $|e| \in [0,1]$ were generated by setting parameters as $\alpha = 0.5$ and $\delta = 0.1$. Significant differences were observed, as illustrated in Fig 5.

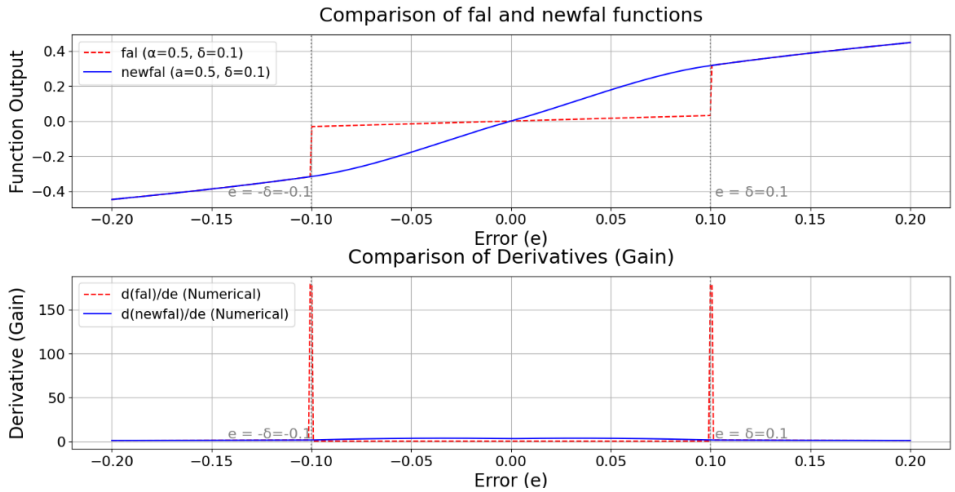

Fig. 5 Comparison of fal and newfal functions and their first-order derivatives (smoothness analysis)

It was seen from Fig 5 that the *fal* function exhibited significant value jumps near $|e| = \delta$, which violated the basic continuity condition, making it discontinuous in C^0 sense. In addition, its first derivative showed sharp peaks at switching point, indicating a lack of C^1 smoothness. In practical control signals, such singularities give rise to instantaneous large-amplitude changes, with the possibility of causing high-frequency chattering.

On the other hand, the *newfal* function was constructed using piecewise polynomials, ensuring both function value and derivative continuity at junction points, achieving C^1 smoothness. Graphical analyses confirmed the smooth transition of the newfal function smooth transition near $|e| = \delta$, effectively eliminating abrupt gain changes. This characteristic provided the controller with more stable feedback regulation capability and theoretically reduced chattering probability.

When *newfal* replaced *fal* within an otherwise identical control framework, the system exhibited smoother control behaviors without altering control intensity.

This improvement offered a structurally grounded performance enhancement without adding computational complexity.

A standard second-order plant model was developed, expressed as:

$$\ddot{x} = -1.5\dot{x} - 2.5x + 1.3u + d(t) \tag{19}$$

The control variable was input signal u, with a disturbance d(t) introduced midway through the simulation to evaluate the dynamic recovery capability of the controller. The control structure adopted a standard second-order ADRC framework, including an ESO and an NLSEF unit. All parameters were conFigured within typical engineering ranges to ensure experimental reproducibility.

The observer was conFigured with a high bandwidth ω_o = 20.0 rad/s, corresponding to parameters β_{01} = 60, β_{02} = 1200, and $_{03}$ = 8000. Controller bandwidth was set to ω_c = 5.0 with a damping ratio of 0.8, resulting in feedback gains of k_p = 25 and k_d = 8. The nonlinear functions *fal* and *newfal* were applied respectively with identical parameters α = 0.5 and δ = 0.05 to ensure a fair comparison.

Simulation duration was 10 s, with a unit step reference applied at t = 0 s and a disturbance injected at t = 5s. Control signal u, system output x, and total disturbance estimate z_3 were recorded for comparative analyses.

Fig 6 shows three groups of key response variables in the simulations. Each set of plots compared system output, control signal, and disturbance estimation under the two nonlinear functions.

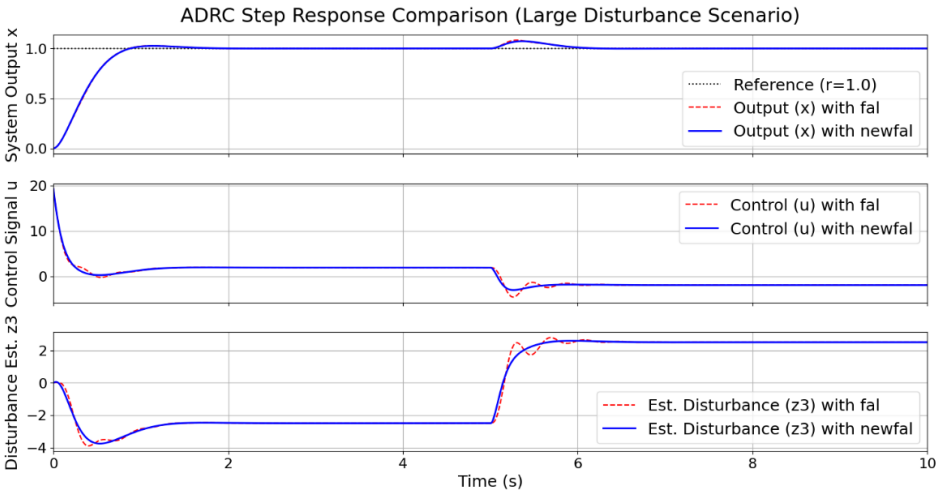

Fig. 6 Comparison of closed-loop ADRC system response using fal and newfal functions under disturbance conditions

System output trajectories under both function structures demonstrated consistent overall behaviors. Under the effect of reference signal, the system

responded rapidly and approached the steady-state value; however, upon disturbance injection, it swiftly recovered without significant overshoot or steady-state error. This indicated that *newfal* could preserve the inherent rapidity and robustness of ADRC system without changing its structural framework, laying a foundation for further improvement in the quality of control signal.

From Fig 6, subFigure 1, it was seen that the overall system output behaviors under both function structures remained essentially consistent. Under the effect of reference signal, the system responded rapidly and approached the steady-state value, while also quickly recovering after disturbance injection. No significant overshoot or steady-state error was observed. This indicated that the use of *newfal* function preserved the inherent rapidity and robustness of the ADRC system without altering the fundamental structure of the controller. It maintained essential performance indicators, thereby laying a solid foundation to further improve control signal quality.

Fig 6, subFigure 2 showed the behavior of the control signal, which served as the core indicator for the evaluation of the effectiveness of smoothness improvements. When the traditional *fal* function was applied, the control output exhibited high-frequency oscillations, characteristic of typical chattering behavior. This phenomenon reflected frequent switching of control direction within small-error region, directly due to function derivative discontinuity. However, the control signal generated by *newfal* was significantly smoother, almost entirely eliminating chattering phenomenon.

This improvement not only positively affected system stability, but also significantly enhanced the lifespan and energy efficiency of the actuator. High-frequency chattering tended to accelerate mechanical wear and tear, while also resulting in unnecessary energy consumption and heat accumulation in electrical control systems. Therefore, the structural optimization brought by *newfal* delivered practical engineering benefits, going beyond a purely theoretical notion of "smoothness."

Fig 6, subFigure 3 further supported the potential advantages of *newfal* in the stability of the dynamic system by analyzing z_3 variable output from ESO. Although both function structures enabled disturbance estimation that closely followed the trend of the actual disturbance, the ESO output driven by *fal* exhibited higher-frequency oscillatory textures, resulting in an estimation behavior with a stronger sense of noise.

On the other hand, z_3 curve driven by *newfal* exhibited smoother variations and clearer trends. This suggested a greater ability for the accurate identification of the evolving trend of disturbances, thereby enhancing the overall reliability and response quality of the observer system. Smoother estimation facilitated more robust error correction decisions by the controller, which became particularly

advantageous under complex disturbance environments with high engineering relevance.

4. Parameter tuning

In control algorithm designs, robustness is typically a primary consideration. One common metric for the assessment of the robustness of a controlled system is maximum sensitivity (Ms). This research employed sensitivity function as the principal criterion for parameter adjustment, ensuring system stability and disturbance rejection capability under varying operating conditions.

Sensitivity function was defined as:

$$S(s)=\frac{1}{1+L(s)} \tag{20}$$

where $L(s)$ is the open-loop transfer function of the system.

Maximum sensitivity, M_s was calculated as:

$$M_s=\max_{0\le\omega<\infty}\left|S(j\omega)\right|=\max_{0\le\omega<\infty}\left|\frac{1}{1+L(j\omega)}\right| \tag{21}$$

Open-loop transfer function, $L_1(s)$, could be derived from $C_1(s)$ and $G_p(s)$ as:

$$L_1(s)=\frac{1}{\lambda_1 s^{\gamma}} \tag{22}$$

where λ_1 and γ are the time constant and the order of the fractional-order low-pass filter in $C_1(s)$ design, respectively. Sensitivity function was calculated as:

$$S(s)=\frac{\lambda_1 s^{\gamma}}{1+\lambda_1 s^{\gamma}} \tag{23}$$

Since γ was a fractional order, when $1<\gamma<2$, the sensitivity magnitude was given by the following equation:

$$\begin{aligned}\left|S(j\omega)\right|&=\left|\frac{\lambda_1(j\omega)^{\gamma}}{1+\lambda_1(j\omega)^{\gamma}}\right|=\left|\frac{\lambda_1\omega^{\gamma}e^{j\frac{\pi}{2}\gamma}}{1+\lambda_1\omega^{\gamma}e^{j\frac{\pi}{2}\gamma}}\right|=\left|\frac{\lambda_1\omega^{\gamma}\left(\cos\left(\frac{\pi}{2}\gamma\right)+j\sin\left(\frac{\pi}{2}\gamma\right)\right)}{\lambda_1\omega^{\gamma}\cos\left(\frac{\pi}{2}\gamma\right)+1+j\lambda_1\omega^{\gamma}\sin\left(\frac{\pi}{2}\gamma\right)}\right|\\&=\frac{\lambda_1\omega^{\gamma}}{\sqrt{\lambda_1^{2}\omega^{2\gamma}+2\lambda_1\omega^{\gamma}\cos\left(\frac{\pi}{2}\gamma\right)+1}}\end{aligned} \tag{24}$$

To find the extremum of Equation (24), the maximum value was achieved when $\omega^{\gamma}=-1/\lambda_1 1\cos(\pi/2\gamma)$. Maximum sensitivity, M_s, was then derived as:

$$M_s = \max_{0\le\omega<\infty}\left|S(j\omega)\right| = \frac{1}{\sqrt{1-\cos^2\left(\frac{\pi}{2}\gamma\right)}} \tag{25}$$

The value of *Ms* ranges from 1.2 to 2.0. Typically, the robustness of controlled system was decreased with the decrease of M_s.

In Equation (22), the amplitude of $L(s)$ was stated as:

$$|\,\mathrm{L}(\mathrm{j}\omega_c)\,| = |\,\mathrm{C}(\mathrm{j}\omega_c)\mathrm{G}_\mathrm{p}(\mathrm{j}\omega_c)\,| = 1 \tag{26}$$

where ω_c is the cutoff frequency of the system.

From Equations (22) and (26), it could be concluded that:

$$\frac{1}{\lambda_1 s^\gamma} = 1 \tag{27}$$

In addition, based on Equations (25) and (27), the parameters for $C_1(s)$ were calculated as:

$$\gamma = \frac{2}{\pi}\arccos\left(-\frac{\sqrt{M_s{}^2-1}}{M_s}\right), \lambda_1 = \frac{1}{\omega_c^\gamma} \tag{28}$$

The parameters γ and λ_1 could be determined based on maximum sensitivity Ms and cutoff frequency ω_c. In addition, the value of λ_2 should be set according to the specific performance requirements of the system.

In ADRC, the primary structure comprised three core modules: TD, ESO, and NLSEF. TD module had relatively few parameters, typically including r, h_0 and h_1. In contrast, ESO and NLSEF modules involved a broader set of parameters: i.e., α_1, α_2, δ, β_1, β_2 and β_3 for ESO and δ_1, β_{01}, β_{02}, k_1 and k_2 for NLSEF.

Due to relative independence of each ADRC module, their parameters could be individually adjusted without interference. This research specifically focused on tuning TD and ESO parameters.

① Parameter adjustment for TD module:

The key parameters of TD included r, h_0 and h_1. Among them, r and h_0 required adjustment. Here, r acted as speed factor, dictating the tracking speed of TD, while h_0 functioned as filtering factor, generally set within the range $h_0=2h_1\sim 10h_1$. h_1, representing the integration step size, affected the noise-filtering capability of the differentiator, with larger values diminishing this capability. Increase of h_0 enhanced the effectiveness of filtering, though excessively high values might compromise tracking accuracy.

② Parameter adjustment for ESO module:

Parameter set for the modified ESO was consistent with that of the traditional ESO, comprising α_1, α_2, δ, β_1, β_2 and β_3. Here, α_1 and α_2 are parameters within local nonlinear function, with commonly assigned values of α_1=0.25 and

α_2=0.5. The value δ defined the interval length of the linear segment, usually set to δ=0.1. The gain coefficients β_1, β_2 and β_3 controlled the responsiveness of the observer, with β_1 and β_2 values were proportional to system rapidity—though excessively high values could cause system divergence. Larger values of β_3 could offset time-delay effects but might also induce oscillations if set too high.

This parameter tuning strategy laid a theoretical foundation for subsequent simulations, ensuring robustness and control precision of the system across various operational conditions.

5. Simulation case study

To verify the superiority of the developed control method compared to existing techniques, a simulation analysis was performed in MATLAB. Benchmark control methods included the fractional-order internal model control (FOIMC) proposed in [19] and improved PID control introduced in [20]. The primary performance evaluation metrics included overshoot (σ%), response time, and the integral of time-weighted absolute error (ITAE). In addition, the robustness of the control methods was evaluated by introducing perturbations in system parameters K and T to explore their performance under varying operating conditions.

Case Study 1: The simulation was based on the permanent magnet synchronous motor (PMSM) speed servo system model according to [19]:

$$G_m(s) = \frac{K}{s(Ts+1)} = \frac{1.52}{s(0.4s+1)} \tag{29}$$

In [19], a fractional-order internal model controller (FOIMC) was developed with the following transfer function:

$$C(s) = \frac{0.4}{1.52 \times 0.03} s^{0.83} + \frac{1}{1.52 \times 0.03 s^{0.17}} \tag{30}$$

To enhance the performance of the system, this research proposed a fractional-order two-degree-of-freedom active disturbance rejection controller (FOADRC), which integrated fractional-order filtering with internal model control. Two controllers were designed to independently handle setpoint tracking and disturbance rejection. The proposed controller were expressed as:

$$C_1(s) = \frac{1}{912 s^{0.222}} \left(10001.52 + \frac{1}{s} + 4000 s \right) \tag{31}$$

$$C_2(s) = \frac{1 + 0.06 s^{1.222}}{1 + 0.063 s^{1.222}} \tag{32}$$

In ADRC framework, the parameters of TD and ESO were set as follows:

TD parameters: r=0.1, h_0=0.1, and h=0.05; ESO parameters: α_1=0.25, α_2=0.5, δ=0.1, β_1=1100, β_2=11000, and β_3=90.

The control method in [19] solely relied on a fractional-order internal model control strategy for two-degree-of-freedom system design. To highlight the advantages of the developed method, this research selected the method in [19] as a benchmark for comparison.

The simulation system input was set as $r(t)$=1(t), with a disturbance applied as $d(t)$=0.1(t-1.5). Comparative control performance between the proposed method and the approach introduced in [19] is illustrated in Fig 7.

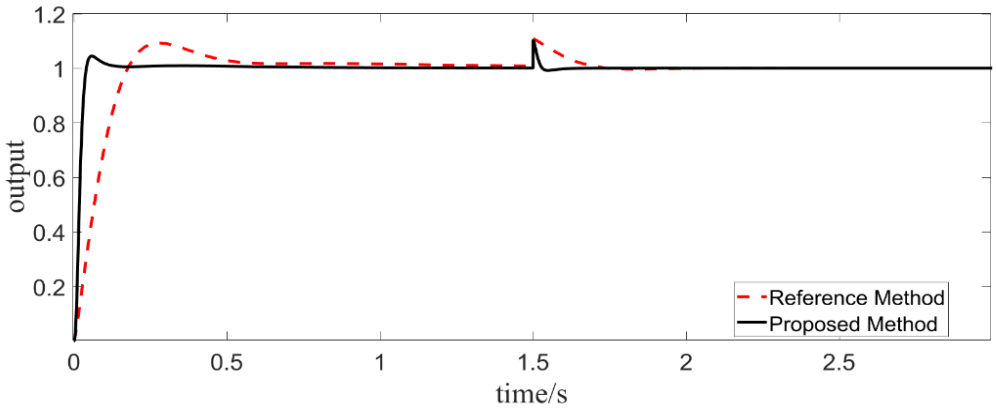

Fig. 7 Unit step response of nominal system

Table 1
Performance parameters of control system

Method	Nominal Model		Model Parameter Perturbation	
	σ%	ITAE	σ%	ITAE
Proposed Method	4.50	0.008	5.02	0.009
Study [19]	5.41	0.020	7.31	0.020

Fig 7 and Table 1 demonstrate that the performance metrics of the proposed method were superior to those of the method proposed in [19], indicating that the developed method exhibited robust control performance. As given in Table 1, under identical initial conditions, the proposed method outperformed the one developed in [19] in terms of overshoot, ITAE, and response time, with a particularly significant improvement in controlling integral time absolute error.

Fig 8 and Table 1 demonstrate the control performance when the controlled system parameters K and T underwent a +30% perturbation, namely K=1.976 and T=0.52. Compared with the method established in [19], the proposed method achieved lower performance parameter values, indicating enhanced robustness. Table 1 further shows that the proposed method exhibited significant improvements in overshoot and ITAE compared to the approach introduced in [19], while maintaining strong robustness under parameter perturbations.

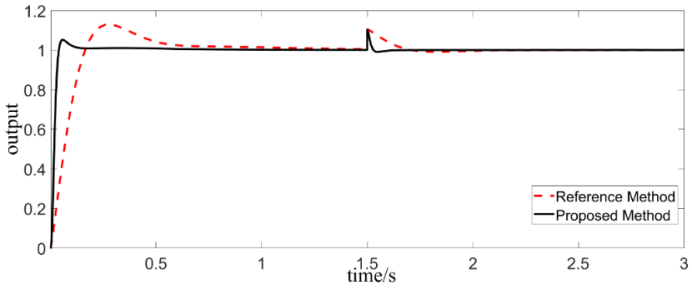

Fig. 8. Unit step response of perturbed system

Example 2: The transfer function of the system in reference [20] was given by:

$$G_m(s)=\frac{K}{s(Ts+1)}=\frac{6.03}{s(0.219s+1)} \tag{33}$$

According to reference [20], with a crossover frequency ω_c=16 rad/s and maximum sensitivity M_s=1.2 in Equation (28), we obtained γ=1.222 and λ_1=0.034. By substituting α=10000 and λ_2=0.035 into Equations (15) and (16), the expression for fractional-order controller was derived as follows:

$$C_1(s)=\frac{1}{2032s^{0.222}}\left(10000.0219+\frac{1}{s}+219s\right) \tag{34}$$

$$C_2(s)=\frac{1+0.034s^{1.222}}{1+0.035s^{1.222}} \tag{35}$$

In ADRC framework, the parameters were set as follows: TD parameters: r=0.1, h_0=0.1, and h=0.05; ESO parameters: α_1=0.25, α_2=0.5, δ=0.1, β_1=1200, β_2=12000, β_3=100, and $r(t)$=1(t).

The simulation system was configured with input $r(t)$=1(t) and disturbance $d(t)$=0.1(t-1.5). The control performance of the proposed method and that of reference [20] are presented in Fig 9 and Fig 10.

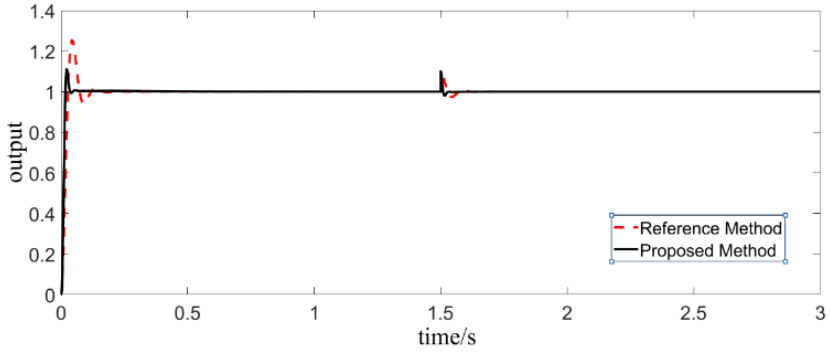

Fig. 9 Unit step response of nominal system

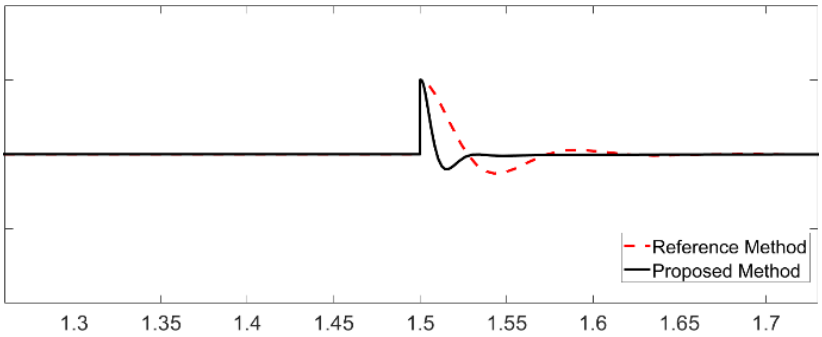

Fig. 10 Partial enlarged drawing

As was seen from Fig 9 and Fig 10, the proposed method exhibited excellent dynamic and steady-state performance. Table 2 indicates that, under both nominal model and parameter perturbation conditions, the ITAE and overshoot (σ%) values of the developed method were lower than those reported in reference [20]; in other words, the algorithm proposed in this research exhibited superior control performance.

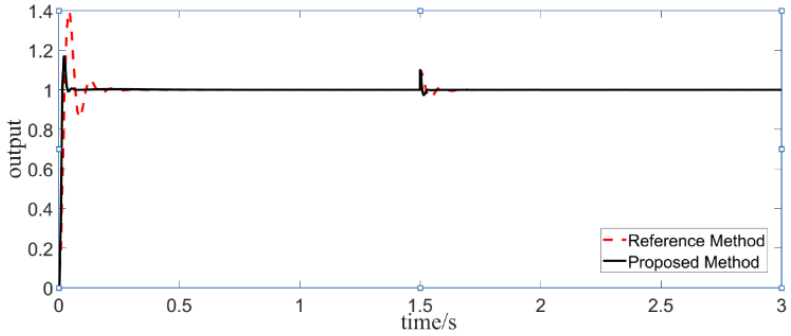

Fig. 11 Unit step response of perturbed system

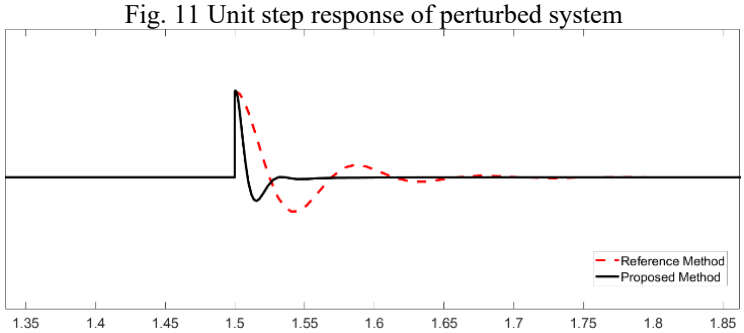

Fig. 12 Partial enlarged drawing of Fig 8

Table 2

Performance parameters of control system

Method	Nominal Model		Model Parameter Perturbation	
	σ%	ITAE	σ%	ITAE
Proposed Method	11.08	0.002	16.85	0.002
Study [20]	25.36	0.005	39.71	0.006

Fig 11 and Fig 12 as well as table 2 present the results when the parameters K and T of the controlled system were perturbed by +50%, i.e., K=9.05 and T=0.033. Compared with the findings of the reference [20], our method demonstrated better control performance and enhanced robustness.

6. Conclusion

This research presented a two-degree-of-freedom fractional-order active disturbance rejection control (FOADRC) strategy to enhance the control performance and robustness of position servo systems. Compared with traditional control methods, the developed approach achieved a balance between system rapidity and disturbance rejection by incorporating fractional-order filters into the internal model control (IMC) and refining the nonlinear function of extended state observer (ESO).

Simulation results indicated that the developed control method significantly outperformed conventional integer-order control methods in terms of overshoot, response time, and the integral of time-weighted absolute error (ITAE) metrics. Notably, under the conditions of parameter perturbations, this approach demonstrated robust resilience, effectively suppressing external disturbances while maintaining system stability and control accuracy.

The novelty of this research lied in the integration of fractional-order control with active disturbance rejection, with a two-degree-of-freedom design to precisely adjust system performance, particularly under complex operating conditions. This method not only improved the dynamic responses of the servo system, but also simplified the parameter tuning process of the controller, making it highly applicable for engineering applications.

Future research could further explore the application of this control strategy in different nonlinear systems and validate it under additional real-world conditions to promote its widespread application in industrial control.

Acknowledgement

This work was supported by the National Natural Science Foundation of China (Grant No. 52405595), the Youth Science Foundation of Shanxi Province (Grant No. 201901D211304), and the Science and Technology Innovation Project of Higher Education Institutions in Shanxi Province (Grant No. 2022L611).

REFERENCES

[1] *Bai Y, Yao J, Hu J, et al.,* Output feedback active disturbance rejection control of an electro-hydraulic servo system based on command filter. Chinese Journal of Aeronautics, 2025, 38(2):103169-103169.

[2] *Su Z, Shi W, Duan J, et al*. Double-loop compensated active disturbance rejection control of electromechanical servo system based on composite disturbance observer. Expert Systems with Applications, 2025, 266126155-126155.
[3] *Akinrinde A H, Ayinde O B, Ferik E S.* Adaptive Position Control of Electrohydraulic Servo Systems with Parameter Uncertainty using Artificial Bee Colony Optimization Algorithm. Asian Research Journal of Mathematics, 2024, 20(10):101-117.
[4] *Li G, Wang H, Liu X, et al.* A sliding mode active disturbance rejection control of DC active power filter for enhancing DC microgrid voltage robustness. Electric Power Systems Research, 2025, 241111388-111388.
[5] *Ibrahim W A, Xu J, Shamma'a A A A, et al*. Intelligent adaptive PSO and linear active disturbance rejection control: A novel reinitialization strategy for partially shaded photovoltaic-powered battery charging. Computers and Electrical Engineering, 2025, 123(PA):110037-110037.
[6] *Luo W, Zhang H, Lian Y*. Enhanced second/third-order hybrid generalized integrator phase-locked loops with linear active disturbance rejection control. Journal of Power Electronics, 2025, 1-11.
[7] *Wu Q, Zhu Q*. Fault-tolerant control of automatic carrier landing using direct lift control based on nonsingular terminal sliding mode and active disturbance rejection control. Transactions of the Institute of Measurement and Control, 2025, 47(1):29-40.
[8] *Yuhang L, Chen W, Haibin D, et al*. Active disturbance rejection heading control of USV based on parameter tuning via an improved pigeon-inspired optimization. Transactions of the Institute of Measurement and Control, 2025, 47(2):304-315.
[9] *Alatawi S K, Zaid A S, Shimy E E M*. Optimal Fractional-Order Controller for Fast Torque Response of an Asynchronous Motor. Processes, 2024, 12(12):2914-2914.
[10] *Wu H, Zhang H, Cui P, et al.* Improved time-delay separation ADRC method for enhancing noise suppression of near-zero magnetic field. Sensors and Actuators: A. Physical, 2025, 387116306-116306.
[11] *Li D, An Z, Zhou Y, et al*. Optimal control of cooling performance using an active disturbance rejection controller for lithium-ion battery packs. Energy, 2025, 322135556-135556.
[12] *Zhang Q, Sun A, Xiao L, et al.* Active disturbance rejection control of pressurizer pressure during startup process in a pressurized water reactor nuclear power plant. Nuclear Engineering and Technology, 2025, 57(4):103325-103325.
[13] *Li Z, Guan X, Liu C, et al*. Active Disturbance Rejection Control Based on Twin-Delayed Deep Deterministic Policy Gradient for an Exoskeleton. Journal of Bionic Engineering, 2025, 1-20.
[14] Fang J, Zheng Q, Zhang H. Nonlinear Robust Control of Turbofan Engine Based on Improved Active Disturbance Rejection Control with Cascade Observer. International Journal of Aeronautical and Space Sciences, 2025, 1-13.
[15] Constantin F, Aquell T A, Mihaela-Elena S. U.P.B. Sci. Bull., Series D, 2018, 80(4): 255-266.
[16] Agila A, Baleanu D, İrfanoğlu B. Optimum controlled fractional order damped oscillatory system. U.P.B. Sci. Bull., Series D, 2025, 87(2): 69-84.
[17] Kaddour G, Hocine B, Zoheir M, et al. Fractional order of Teager Kaiser energy operator for fault diagnosis of rotating machines. U.P.B. Sci. Bull., Series D, 2023, 85(2): 241-252.
[18] Tuan A L. Fuzzy fractional-order control of rubber tired gantry cranes. Mechanical Systems and Signal Processing, 2025, 225112216-112216.
[19] He D, Wang H, Tian Y, et al. Model-free global sliding mode control using adaptive fuzzy system under constrained input amplitude and rate for mechatronic systems subject to mismatched disturbances. Information Sciences, 2025, 697121769-121769.
[20] Zhang ZH, Li J, Wang L, et al. Main Steam Temperature Cascade Control System based on Internal Model Control and Improved Active Disturbance Rejection Control. Proceedings of the CSEE, 2024, 44(23):9331-9341.

[21] *Zhao ZC, Sang H, Zhang JG*., Fractional order Internal Model Control for Speed Servo System of Permanent Magnet synchronous Motor. Journal of System Simulation, 2015, 27(02):384-388.
[22] *Li SY, Zhao ZT, Zhao ZC.,* Improved Internal Model PD-I Control Method for DC Speed Control System of Servo System. Fire Control & Command Control, 2017, 42(07):90-93.